Supporting information

Phytic acid assisted ultra-fast in-situ constructing Ni foam-supported amorphous Ni-Fe phytates to enhance catalytic performance for oxygen evolution reaction

Taotao Gao,[a] * Shuaiwei Wu,[b] Xiaoqin Li,[a] Chaohong Lin,[c] Qu Yue,[d] Xiangmin Tang,[b] Shumin Yu,[b] and Dan Xiao [a, d] *

a Institute for Advanced Study, Chengdu University, Chengdu 610106, P. R. China.

b School of Mechanical Engineering, Chengdu University, Chengdu 610106, P. R. China.

c Southwest Institute of Chemical Co., Ltd., Chengdu 610225, P. R. China.

d College of Chemistry, Sichuan University, Chengdu 610064, P. R. China.

* Corresponding author: Taotao Gao and Dan Xiao

Tel number: +86-28-85415029

Fax number: +86-28-85416029

E-mail address: gaott1011@outlook.com (Taotao Gao) and xiaodan@scu.edu.cn (Dan Xiao)

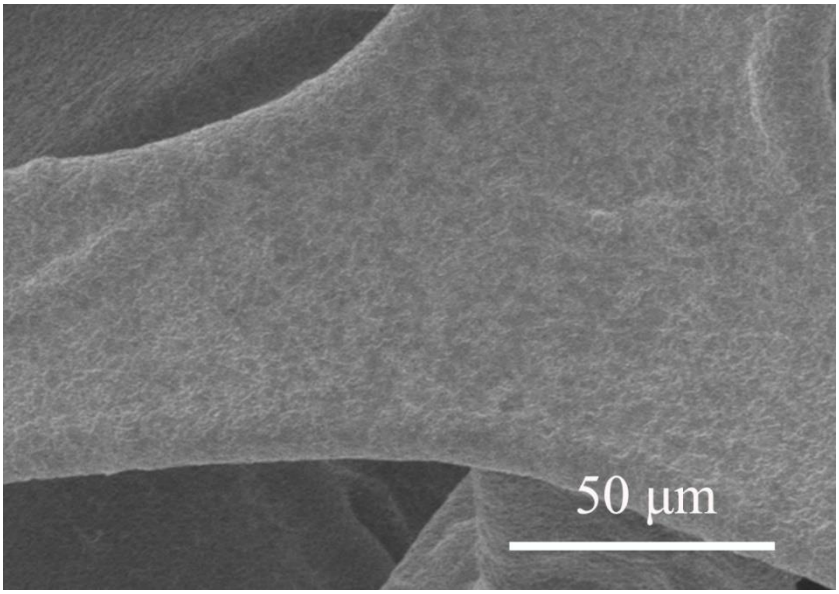

Fig. S1 SEM image of the Ni-Fe-phy@NF.

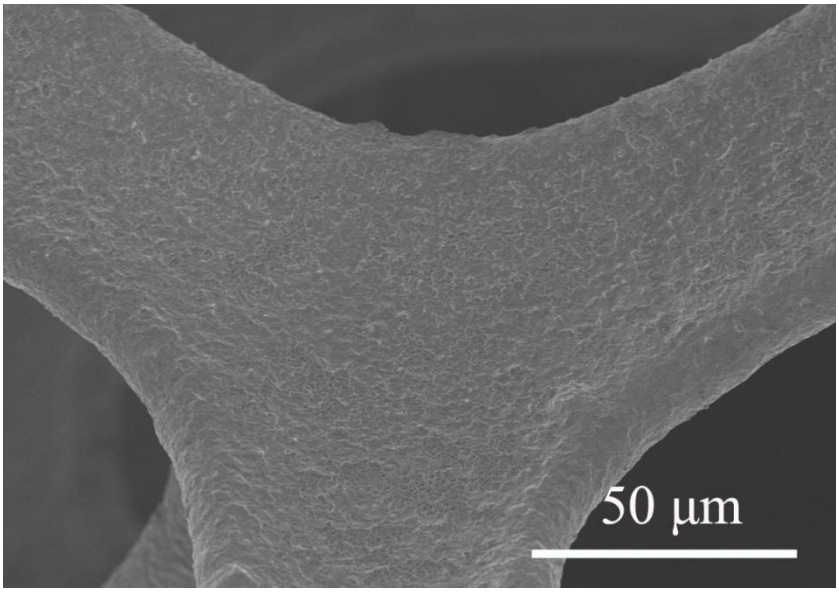

Fig. S2 SEM image of the Ni-Fe-pho@NF.

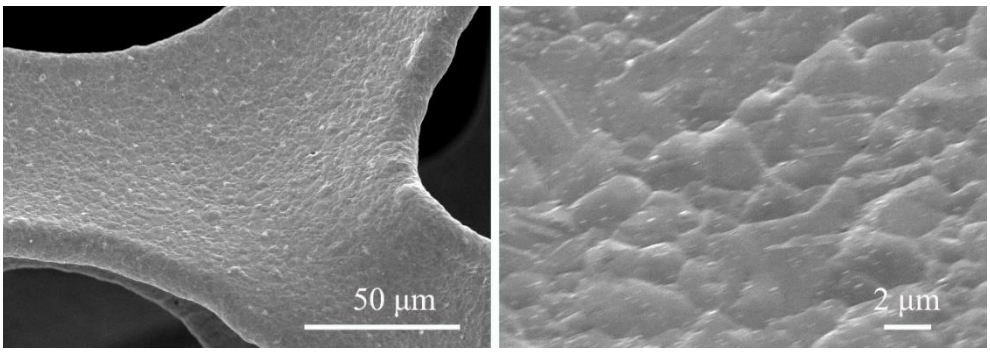

Fig. S3 SEM images of the Ni-phy@NF.

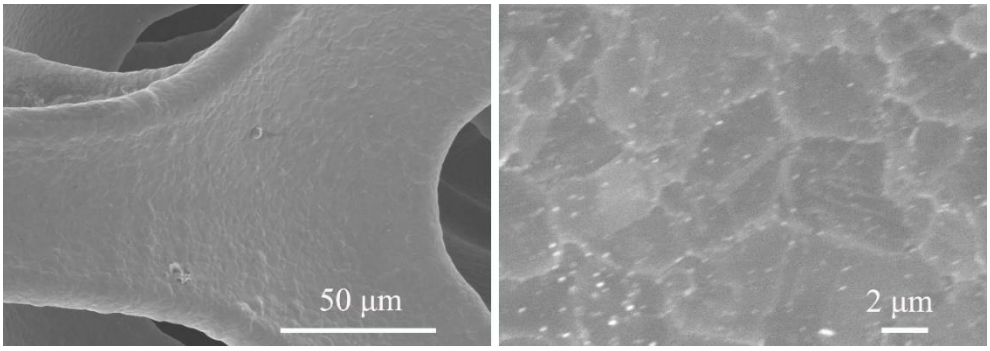

Fig. S4 SEM images of the Ni-pho@NF.

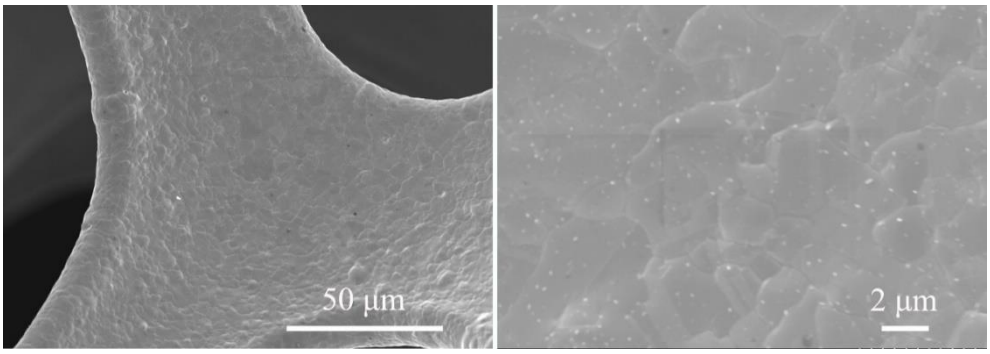

Fig. S5 SEM images of the NF.

Table S1. Hydrogen ion concentrations in the etching solutions.

Etching solution	Phytic acid (0.6 mol L^{-1})	Phytic acid (0.6 mol L^{-1}) containing Fe (3+) (0.5 mol L^{-1})	Phosphoric acid (0.6 mol L^{-1})	Phosphoric acid (0.6 mol L^{-1}) containing Fe (3+) (0.5 mol L^{-1})
H^+ concentration (mol L^{-1})	1.04	2.88	0.09	1.10

Table S2. Element content of Fe and P in Ni-Fe-phy@NF and Ni-Fe-pho@NF according to the ICP-OMS test.

Catalytic electrode	Ni-Fe-phy@NF	Ni-Fe-pho@NF
Fe (wt%)	0.16%	0.13%
P (wt%)	0.54%	0.09%

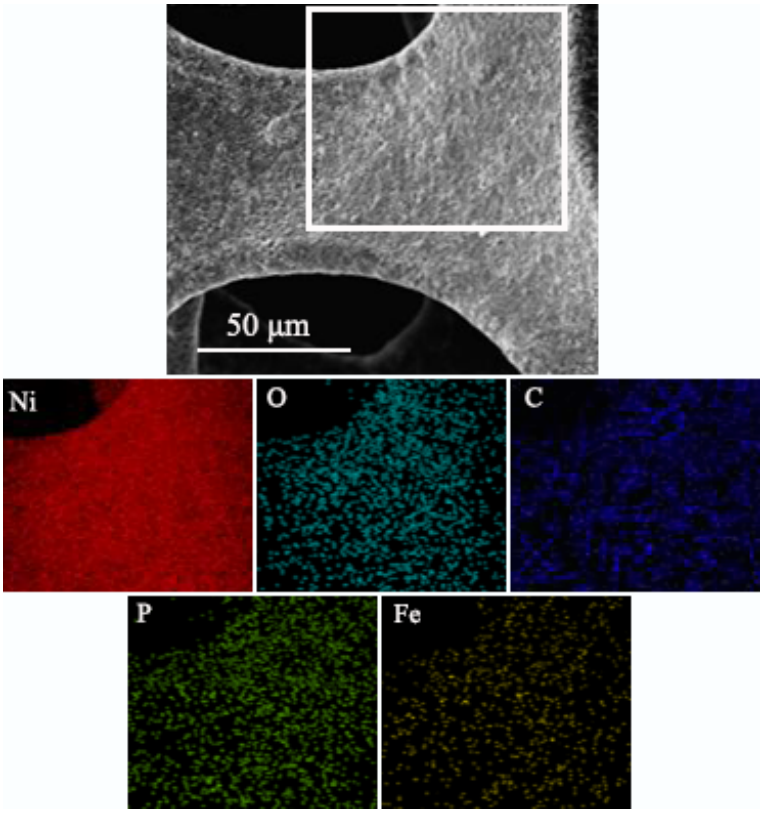

Fig. S6 SEM image of Ni-Fe-phy@NF and the element mapping of Ni, O, C, P and Fe, respectively.

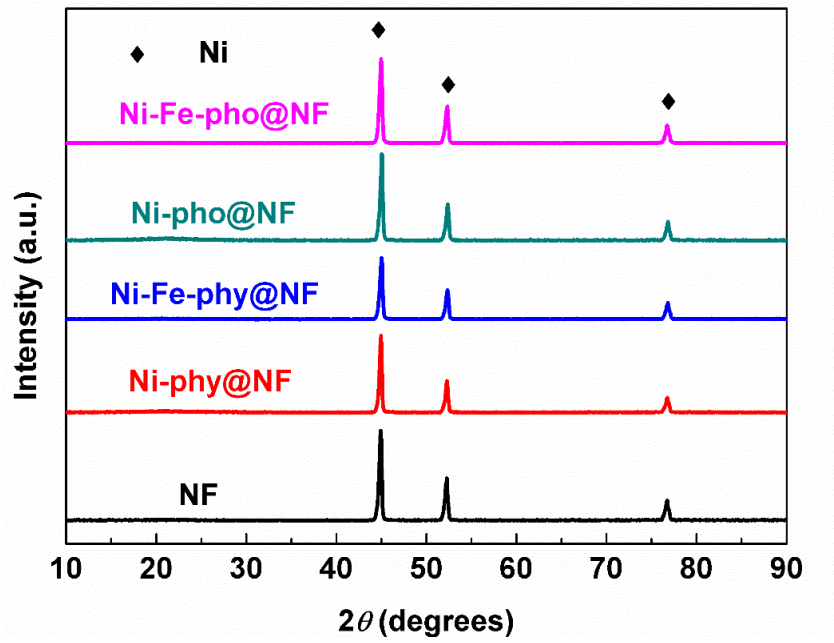

Fig. S7 XRD patterns of the prepared catalytic electrodes.

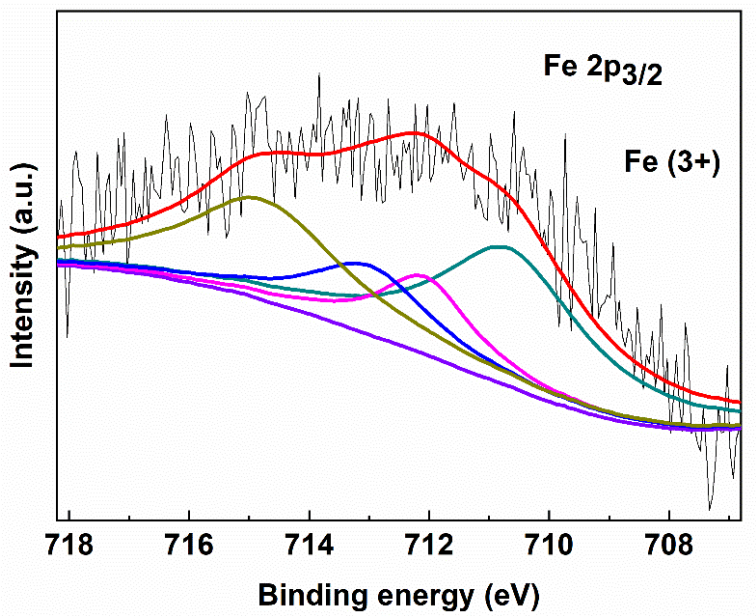

Fig. S8 Fe $2p_{3/2}$ XPS spectrum of the Ni-Fe-phy@NF.

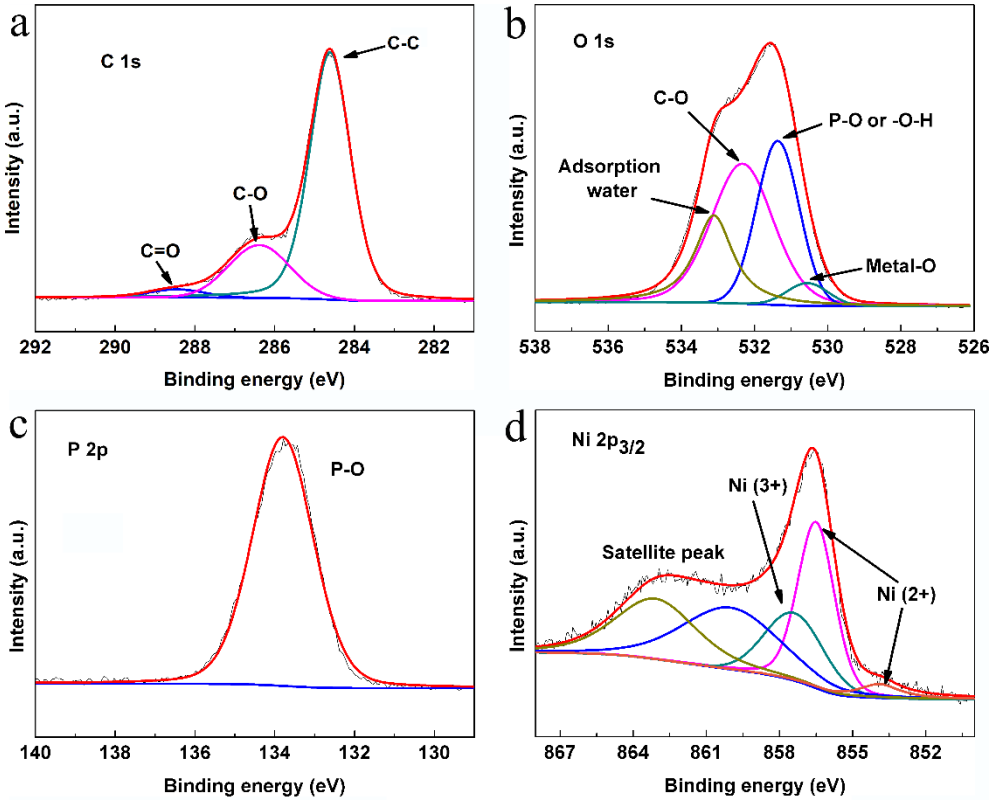

Fig. S9 a) C 1s, b) O 1s, c) P 2p and d) Ni $2p_{3/2}$ XPS spectra of the Ni-phy@NF.

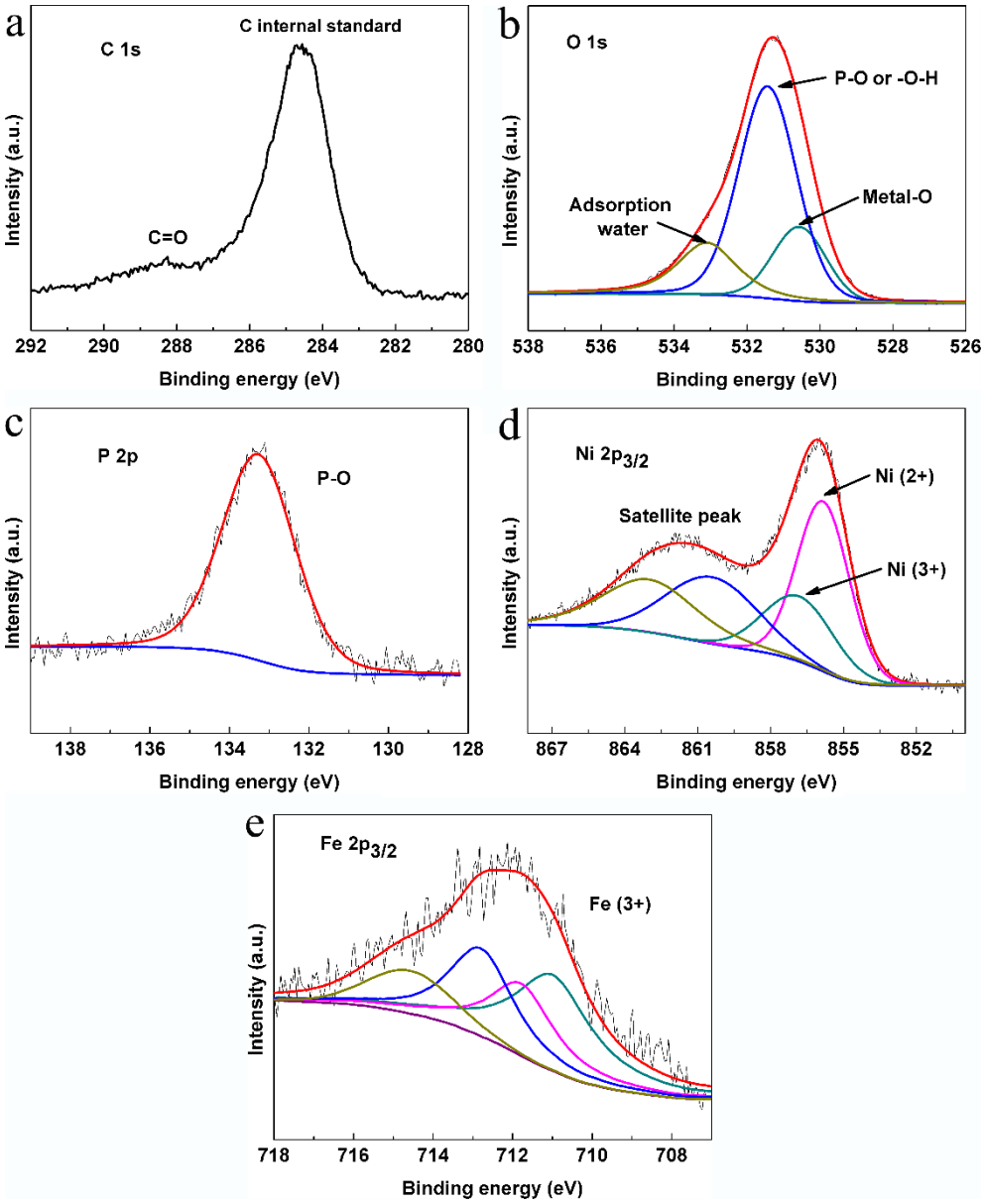

Fig. S10 a) C 1s, b) O 1s, c) P 2p, d) Ni $2p_{3/2}$ and e) Fe $2p_{3/2}$ XPS spectra of the Ni-Fe-pho@NF.

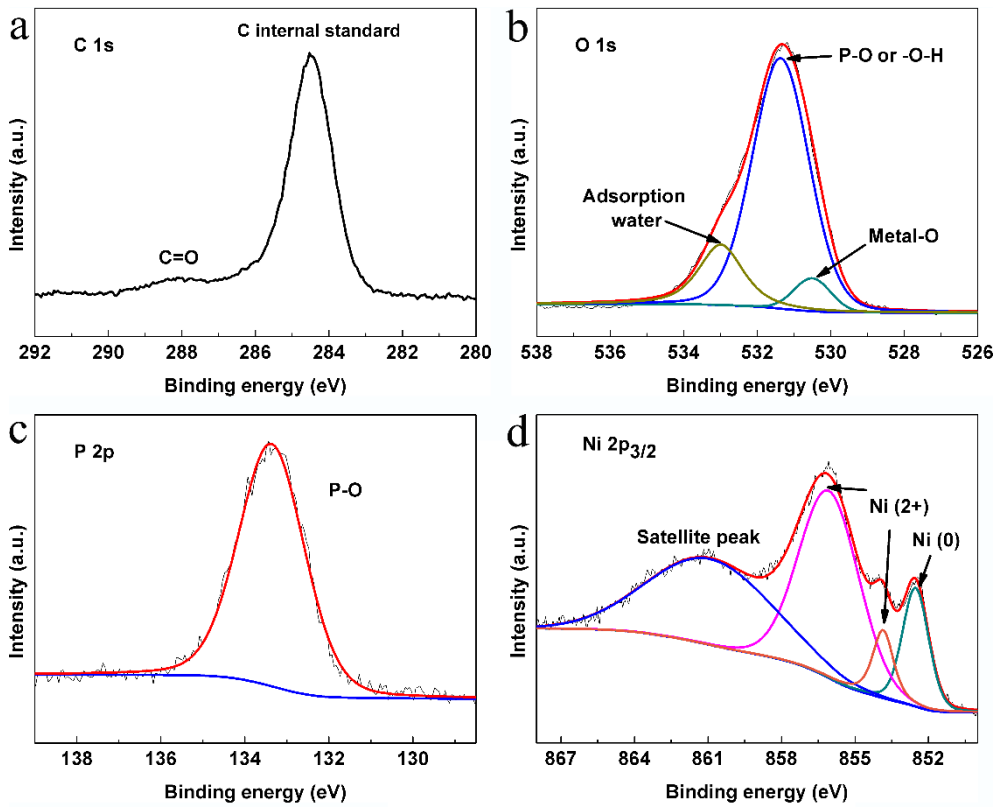

Fig. S11 a) C 1s, b) O 1s, c) P 2p and d) Ni $2p_{3/2}$ XPS spectra of the Ni-pho@NF.

Table S3. According to the XPS spectra, the Ni (3+) content in Ni-Fe-phy@NF, Ni-Fe-pho@NF, Ni-phy@NF and Ni-pho@NF.

	Ni (%)	
Chemical environment	Ni (2+)	Ni (3+)
Ni-Fe-phy@NF	62.2	37.8
Ni-Fe-pho@NF	66.6	33.4
Ni-phy@NF	65.5	34.5
Ni-pho@NF	100	0

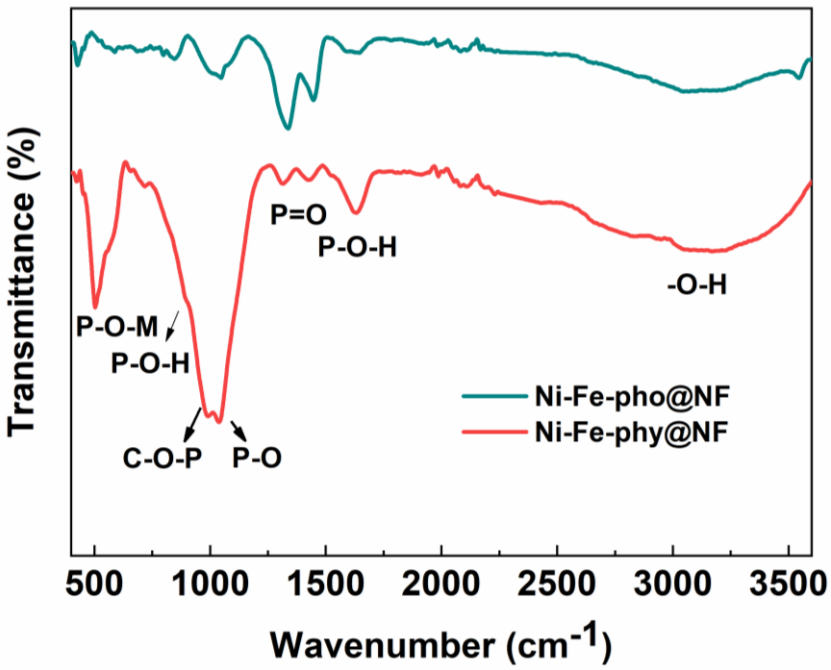

Fig. S12 The ATR-IR of Ni-Fe-phy@NF and Ni-Fe-pho@NF.

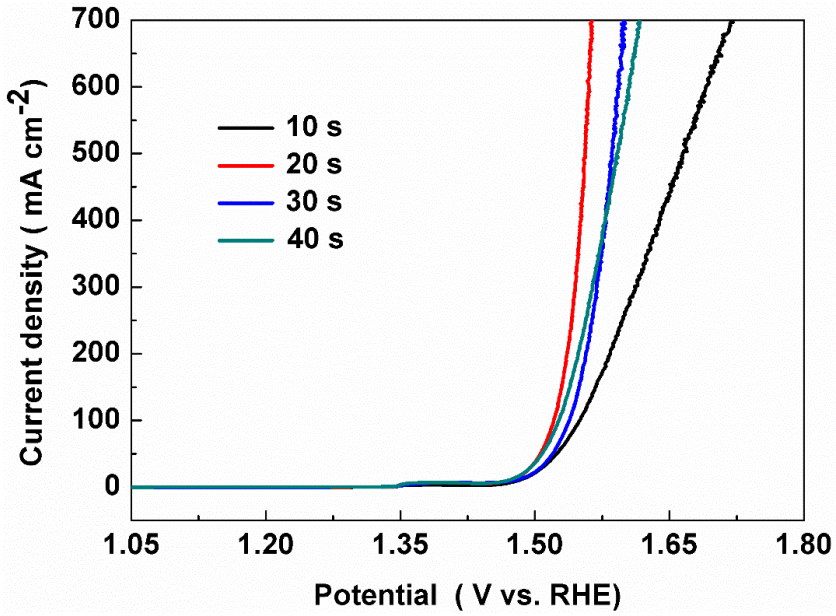

Fig. S13 Polarization curves of the Ni-Fe-phy@NF electrodes based on different reaction time during preparation process.

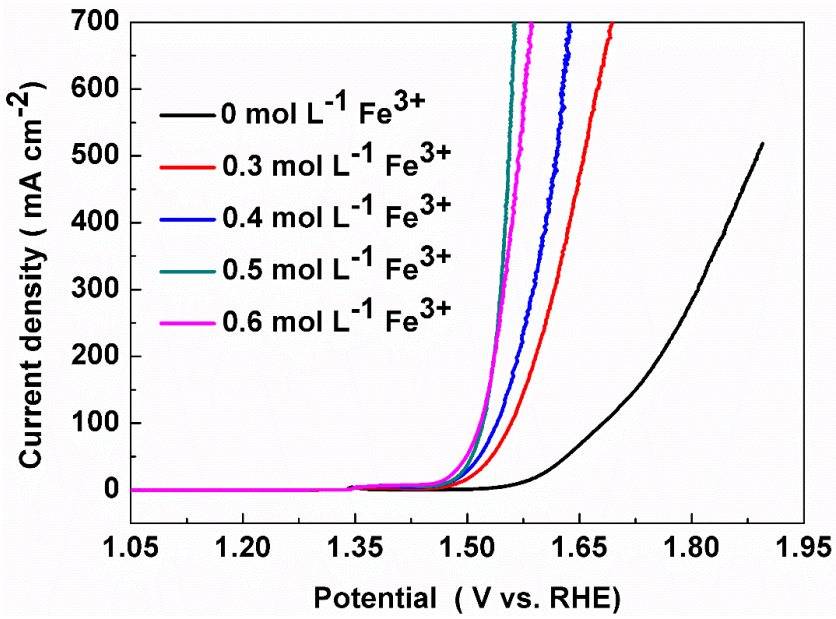

Fig. S14 Polarization curves of the Ni-Fe-phy@NF electrodes based on different Fe^{3+} concentrations in the etching solutions during preparation process.

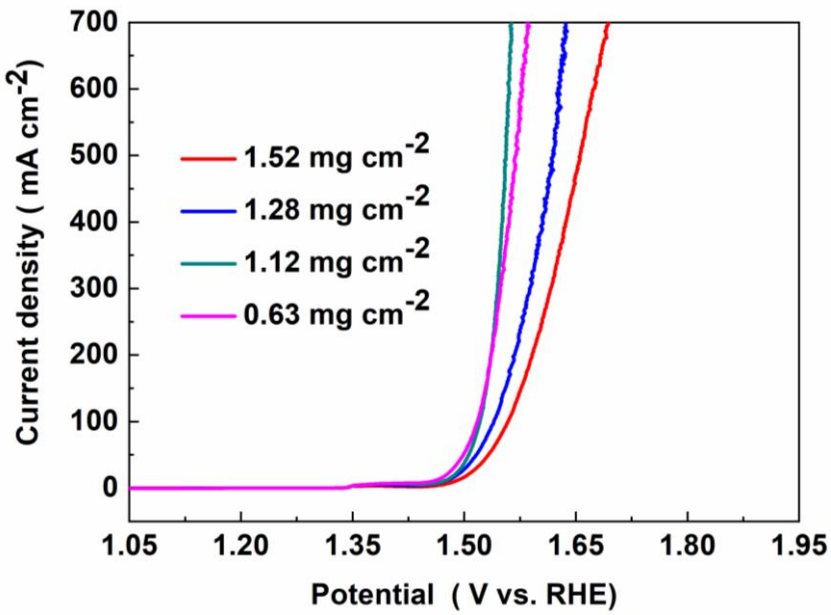

Fig. S15 Polarization curves of the Ni-Fe-phy@NF electrodes with different loading mass via adjusting the Fe^{3+} concentrations in the etching solutions during preparation process.

The Ni-Fe-phy@NF electrodes with different loading mass are obtained by adjusting the Fe concentration in the preparation solution (0.6, 0.5, 0.4 and 0.3 mol L^{-1}), and the corresponding loading mass is 0.63, 1.12, 1.28 and 1.52 mg cm^{-2}, respectively. The Ni-Fe-phy@NF shows the highest catalytic activity at the loading mass of 1.12 mg cm^{-2}.

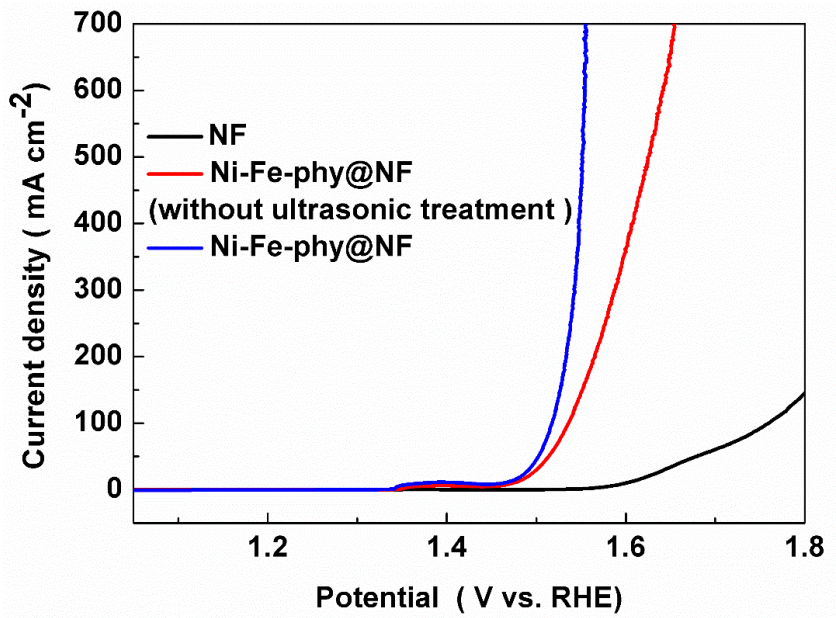

Fig. S16 Polarization curves of the NF, Ni-Fe-phy@NF without ultrasonic treatment and Ni-Fe-phy@NF electrode.

Table S4. Comparison of OER catalytic activity in 1 M KOH.

Catalysts	Collector	Tafel slope (mV dec $^{-1}$)	Overpotential (mV) at different current density (mA cm^{-2})			Main preparation processes	References
			10	100	200		
$Fe_{0.2}Ni_{0.8}$/NC-600-a	Glassy carbon electrode	76	~270	~400	-	Water bath (30°C, 18 h) Calcination (600°C, 3h)	[1]
$Ni_{4/5}Fe_{1/5}$-LDHs-S-2	Glassy carbon electrode	61.5	257	-	-	Hydrothermal Reaction (120°C, 12h)	[2]
Ni@Ru/CNS-10%	Nickel foam	35	255	289	~310	Hydrothermal Reaction (120°C, 24h) Calcination (400°C, 2h)	[3]
$Ni_{1.25}Ru_{0.75}P$	Carbon cloth	50	260	~315	~330	Electrodeposition (-)	[4]
P-FeNiO/CNS	Glassy carbon electrode	52.2	220	~290	-	Calcination (300°C, 3h)	[5]
NiFe-LDH-ZnO(2min)	Nickel foam	57	210	~370	-	Hydrothermal Reaction (130°C, 12h) Plasma magnetron sputtering (2min)	[6]
$Ni^{vac}Fe^{vac}$-LDH	Carbon paper	52	230	~350	~440	Hydrothermal Reaction (150°C, 6h) Etching process (160°C, 3h)	[7]
$FeOOH_{xnm}$/Ni-Fe LDH	Glassy carbon electrode	27	174	-	-	Hydrothermal Reaction (120°C, 6h)	[8]
$NiFe_x/NiFe_2O_4$ @NC	Carbon paper	51.4	262	~310	~320	Calcination (600°C, 2h, 350, 0.5h)	[9]
NiFe LDH-$Ni_{(III)}$Li	NiFeMo alloy	35	248	~290	-	Oil bath (170°C 5h)	[10]
Ni-Fe-phy@NF	Nickel foam	48	233	287	303	Ultrasonic treatment (20 s)	This work

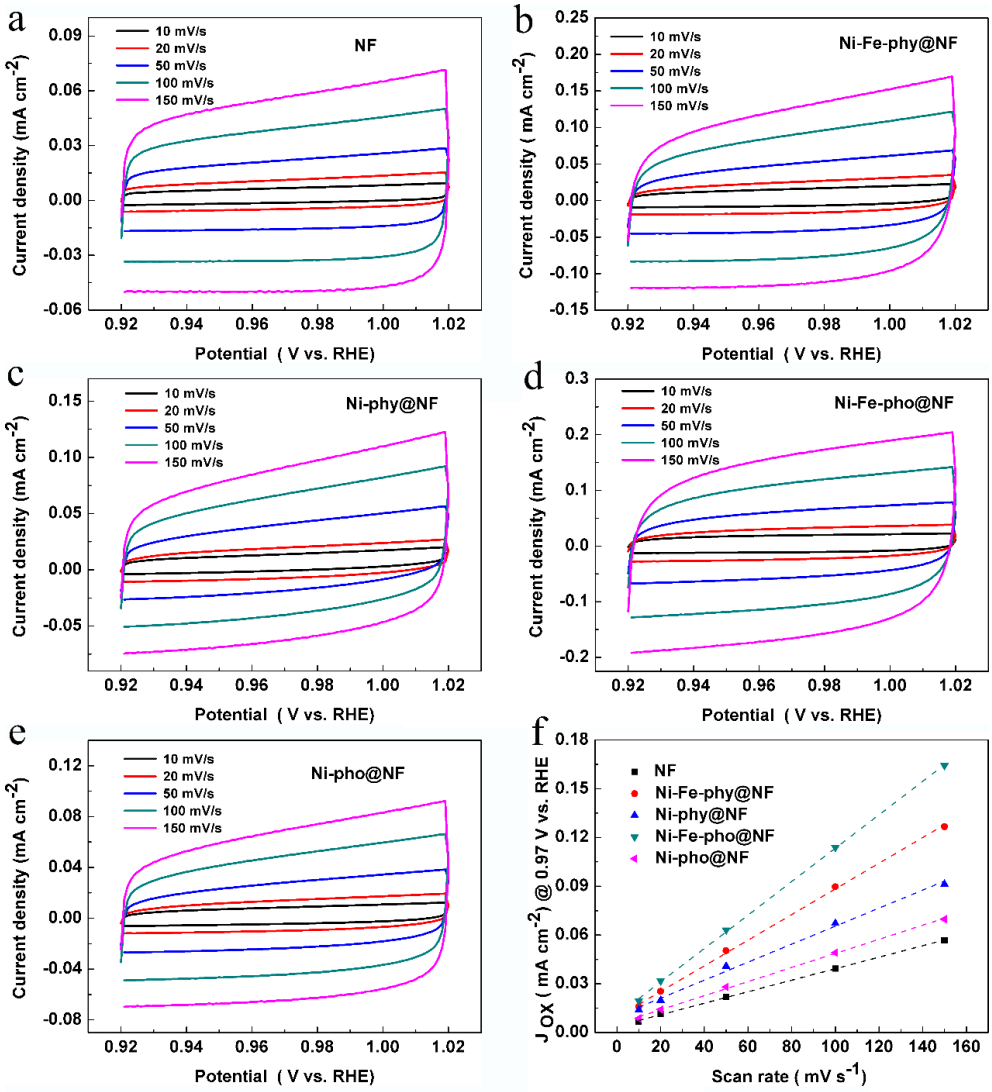

Fig. S17 Double-layer capacitance measurements of these catalytic electrodes; a-e) the cyclic voltammograms of the catalysts at a series of scan rates of 10, 20, 50, 100 and 150 mV s^{-1} from 0.92 to 1.02 V vs. RHE in 1 M KOH; f) the linear fitting of the oxidation currents of the catalysts at 0.97 V vs. RHE versus scan rates.

Electrical double-layer capacitance measurements were used to determine electrochemical active surface area of the catalysts. According to Fig. S17f, the electrical double-layer capacitance could be obtained. Then the electrochemical active surface area could be obtained based on the specific capacitance value of a smooth standard with a real surface area of 1 cm^{-2}. 40 μF cm^{-2} is considered as the value of specific capacitance for a smooth standard with a real surface area of 1 cm^{-2} based on previous studies.[11]

The electrochemical active surface area could be obtained via the following equation:

$$A_{ECSA}=\frac{\text{The electrical double-layer capacitor}}{40}$$

For example:

$$\text{Ni-Fe-phy@NF: } A_{ECSA}=\frac{789.3}{40}=19.7\ cm^2_{ECSA}$$

Table S5. Calculated electrochemical active surface area (ECSA) of the obtained electrodes.

Catalysts	NF	Ni-Fe-phy@NF	Ni-phy@NF	Ni-Fe-pho@NF	Ni-pho@NF
Specific Capacitance (μF cm^{-2})	354.4	789.3	554.5	1030.0	433.7
ECSA (cm^2_{ECSA})	8.9	19.7	13.9	25.8	10.8

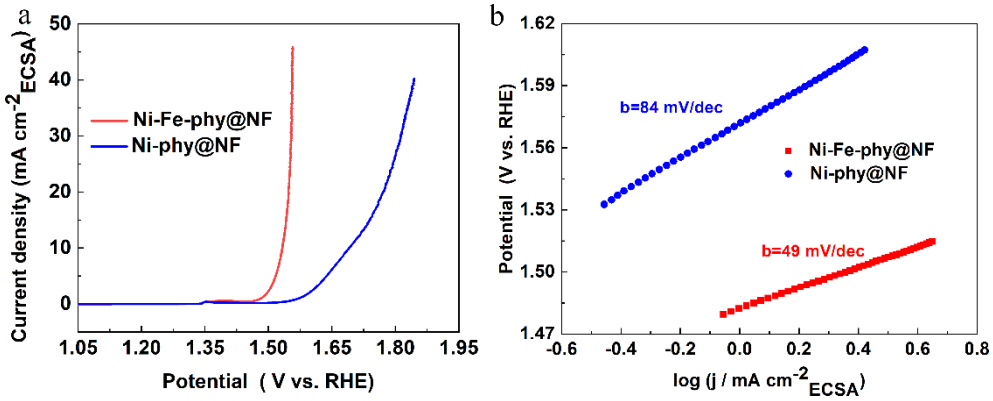

Fig. S18 a) The polarization curves normalized to the electrochemically active surface area and b) the corresponding Tafel plots of Ni-Fe-phy@NF and Ni-phy@NF.

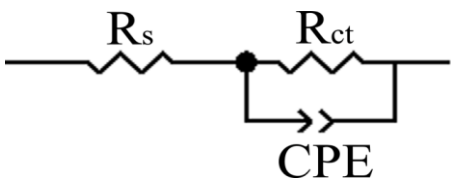

Fig. S19 Equivalent circuit for the test of the electrochemical impedance spectroscopy.

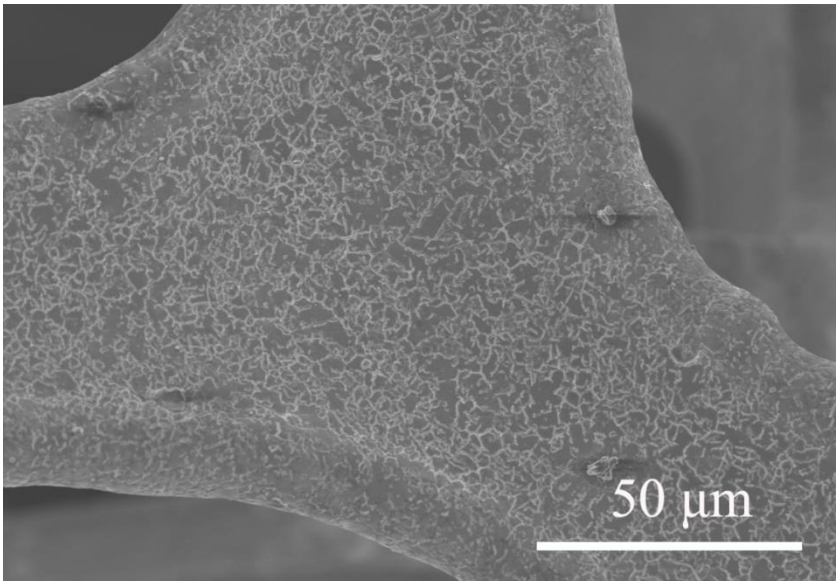

Fig. S20 SEM image of Ni-Fe-phy@NF after OER process.

Table S6. Content of P and Fe in Ni-Fe-phy@NF after OER process and Ni-Fe-pho@NF after OER process according to the ICP-OMS test

Catalytic electrode	Ni-Fe-phy@NF after OER process	Ni-Fe-pho@NF after OER process
Fe(wt%)	0.15	0.11
P(wt%)	0.21	0.00

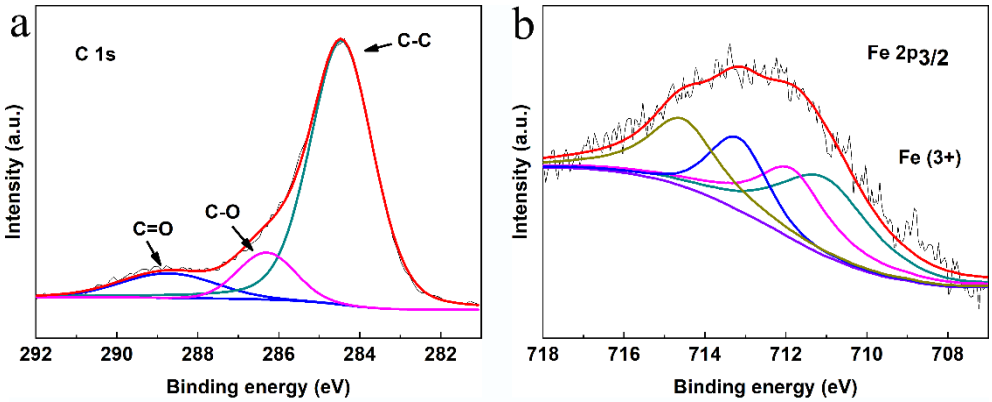

Fig. S21 a) C1s and b) Fe $2p_{3/2}$ XPS spectrum of the Ni-Fe-phy@NF after OER process.

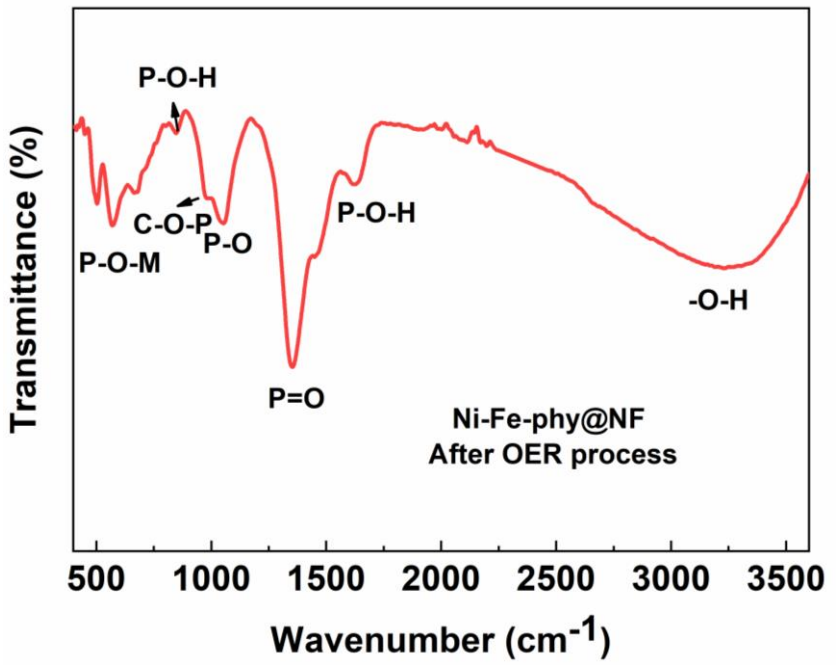

Fig. S22 The ATR-IR spectrum of Ni-Fe-phy@Ni after OER process

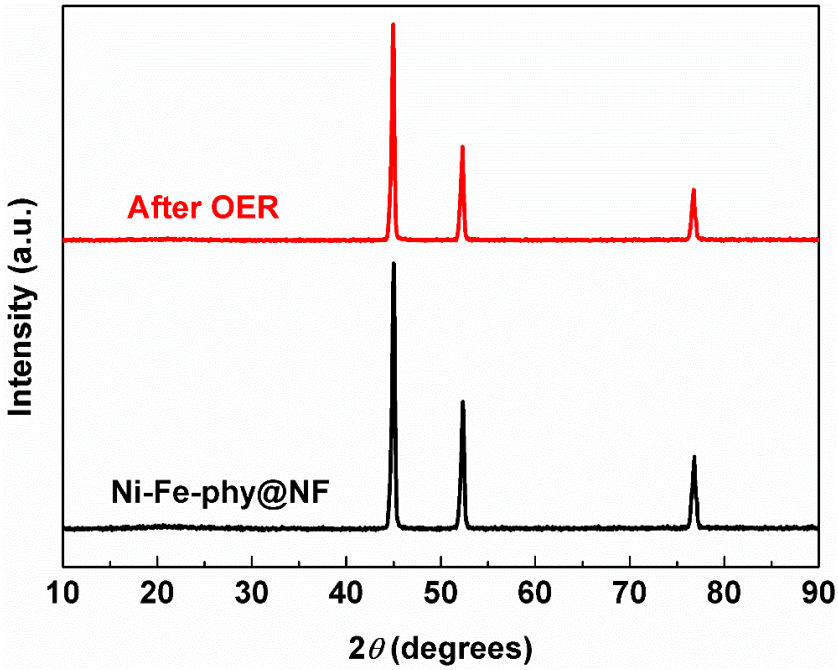

Fig. S23 XRD patterns of the Ni-Fe-phy@NF electrode before and after OER process.

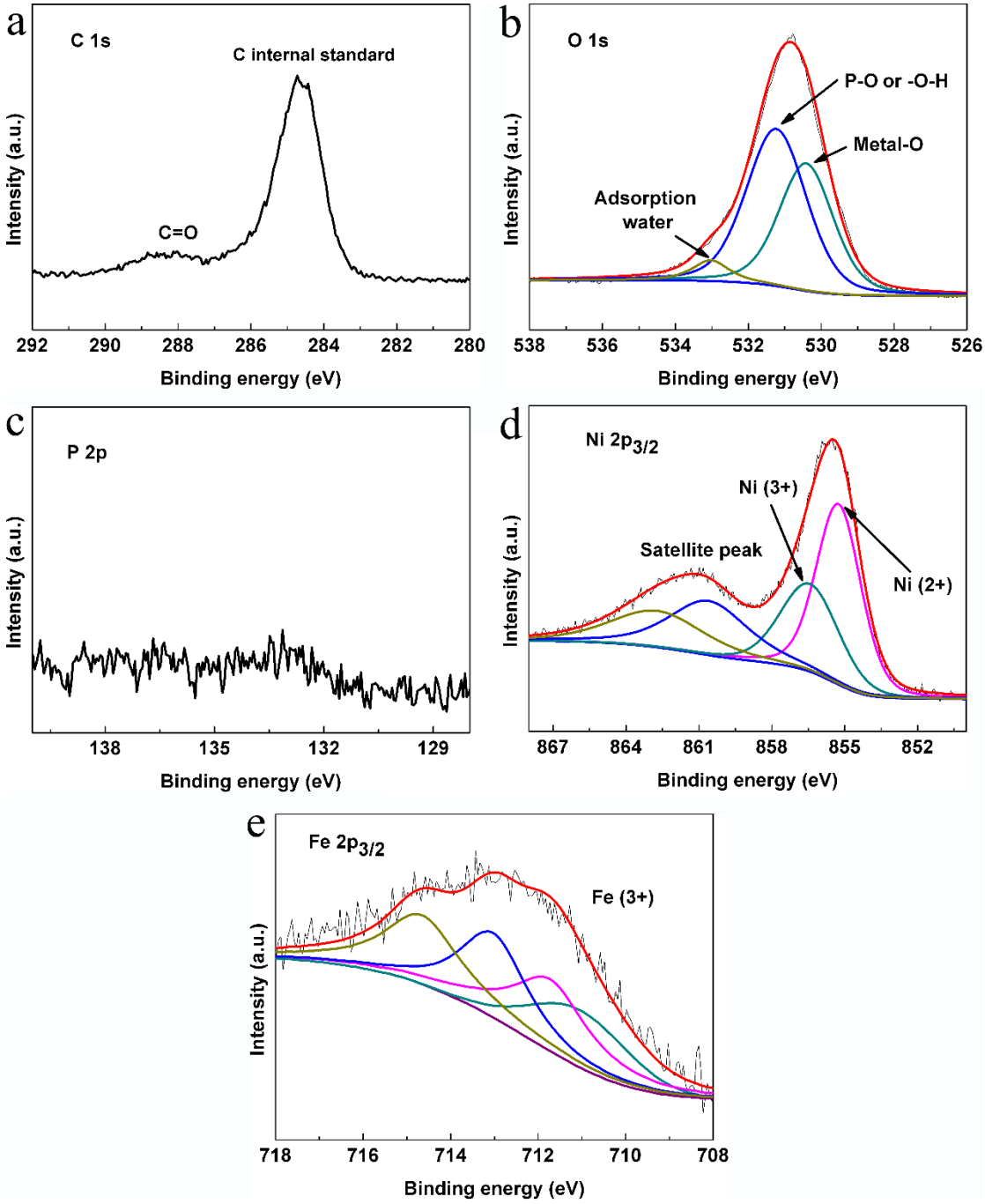

Fig. S24 a) C 1s, b) O 1s, c) P 2p, d) Ni $2p_{3/2}$ and e) Fe $2p_{3/2}$ XPS spectra of the Ni-Fe-pho@NF after OER process.

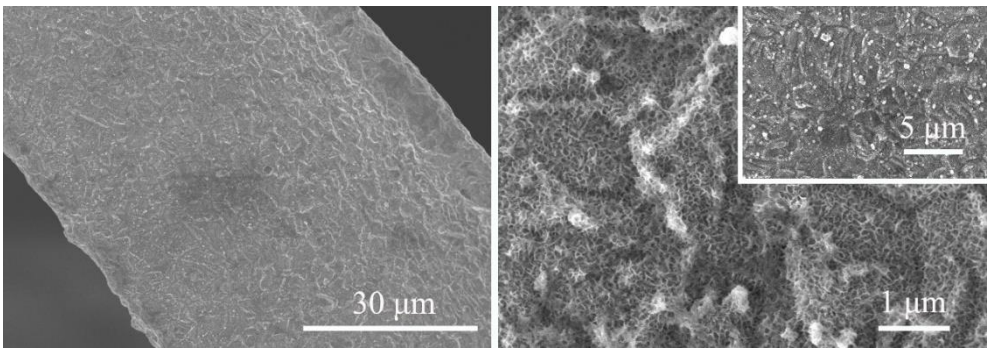

Fig. S25 SEM image of Ni-Fe-pho@NF after OER process.

Table S7. According to the XPS spectra, the Ni (3+) content in Ni-Fe-phy@NF and Ni-Fe-pho@NF after OER process.

	Ni (%)	
Chemical environment	Ni (2+)	Ni (3+)
Ni-Fe-phy@NF after OER process	57.3	42.7
Ni-Fe-pho@NF after OER process	61.9	38.1

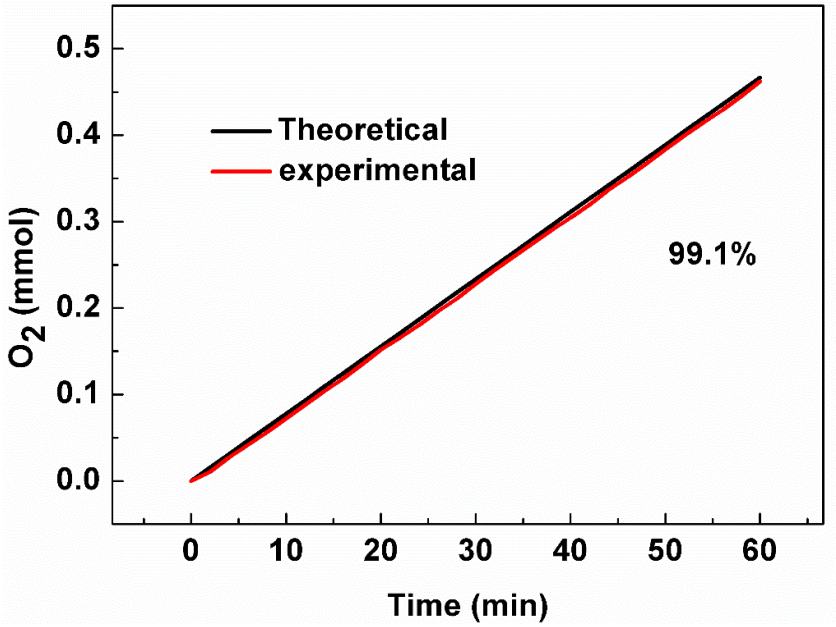

Fig. S26 Faraday efficiency of the Ni-Fe-phy@NF at the current density of 50 mA cm^{-2}.

References

[1] Y. Zhou, Y. Li, L. Zhang, L. Zhang, L. Li, J. Tian, M. Wang, J. Xu, B. Dai, Y. Li, Fe-leaching induced surface reconstruction of Ni-Fe alloy on N-doped carbon to boost oxygen evolution reaction, Chemical Engineering Journal, 394 (2020) 124977.

[2] S. Li, J. Liu, S. Duan, T. Wang, Q. Li, Tuning the oxygen evolution electrocatalysis on NiFe-layered double hydroxides via sulfur doping, Chinese Journal of Catalysis, 41 (2020) 847-852.

[3] Y. Li, G. Zhang, W. Lu, F. Cao, Amorphous Ni-Fe-Mo Suboxides Coupled with Ni Network as Porous Nanoplate Array on Nickel Foam: A Highly Efficient and Durable Bifunctional Electrode for Overall Water Splitting, Advanced Science, 7 (2020) 1902034.

[4] M. Chen, S. Lu, X. Fu, J. Luo, Core-Shell Structured NiFeSn@NiFe (Oxy)Hydroxide Nanospheres from an Electrochemical Strategy for Electrocatalytic Oxygen Evolution Reaction, Advanced Science, 7 (2020) 1903777.

[5] Z. Liu, B. Tang, X. Gu, H. Liu, L. Feng, Selective structure transformation for NiFe/$NiFe_2O_4$ embedded porous nitrogen-doped carbon nanosphere with improved oxygen evolution reaction activity, Chemical Engineering Journal, 395 (2020) 125170.

[6] Y. Luo, Y. Wu, D. Wu, C. Huang, D. Xiao, H. Chen, S. Zheng, P.K. Chu, NiFe-Layered Double Hydroxide Synchronously Activated by Heterojunctions and Vacancies for the Oxygen Evolution Reaction, ACS Applied Materials & Interfaces, 12 (2020) 42850-42858.

[7] L. Peng, N. Yang, Y. Yang, Q. Wang, X. Xie, D. Sun-Waterhouse, L. Shang, T. Zhang, G.I.N. Waterhouse, Atomic Cation-Vacancy Engineering of NiFe-Layered Double Hydroxides for Improved Activity and Stability towards the Oxygen Evolution Reaction, Angewandte Chemie International

Edition, 60 (2021) 24612-24619.
[8] J. Chen, F. Zheng, S. Zhang, A. Fisher, Y. Zhou, Z. Wang, Y. Li, B. Xu, J. Li, S. Sun, Interfacial Interaction between FeOOH and Ni-Fe LDH to Modulate the Local Electronic Structure for Enhanced OER Electrocatalysis, ACS Catalysis, 8 (2018) 11342-11351.
[9] J. Zhao, X. Zhang, M. Liu, Y. Jiang, M. Wang, Z. Li, Z. Zhou, Metal-organic-framework-derived porous 3D heterogeneous $NiFe_x/NiFe_2O_4$@NC nanoflowers as highly stable and efficient electrocatalysts for the oxygen-evolution reaction, Journal of Materials Chemistry A, 7 (2019) 21338-21348.
[10] Z. Xu, Y. Ying, G. Zhang, K. Li, Y. Liu, N. Fu, X. Guo, F. Yu, H. Huang, Engineering NiFe layered double hydroxide by valence control and intermediate stabilization toward the oxygen evolution reaction, Journal of Materials Chemistry A, 8 (2020) 26130-26138.
[11] Y. Liu, N. Ran, R. Ge, J. Liu, W. Li, Y. Chen, L. Feng, R. Che, Porous Mn-doped cobalt phosphide nanosheets as highly active electrocatalysts for oxygen evolution reaction, Chemical Engineering Journal, 425 (2021) 131642.